Progressive sheet-to-tubule transformation is a general mechanism for endoplasmic reticulum partitioning in dividing mammalian cells

Maija Puhka*, Merja Joensuu*, Helena Vihinen, Ilya Belevich, and Eija Jokitalo
Electron Microscopy Unit, Institute of Biotechnology, University of Helsinki, 00014 Helsinki, Finland

ABSTRACT **The endoplasmic reticulum (ER) is both structurally and functionally complex, consisting of a dynamic network of interconnected sheets and tubules. To achieve a more comprehensive view of ER organization in interphase and mitotic cells and to address a discrepancy in the field (i.e., whether ER sheets persist, or are transformed to tubules, during mitosis), we analyzed the ER in four different mammalian cell lines using live-cell imaging, high-resolution electron microscopy, and three dimensional electron microscopy. In interphase cells, we found great variation in network organization and sheet structures among different cell lines. In mitotic cells, we show that the ER undergoes both spatial reorganization and structural transformation of sheets toward more fenestrated and tubular forms. However, the extent of spatial reorganization and sheet-to-tubule transformation varies among cell lines. Fenestration and tubulation of the ER correlates with a reduced number of membrane-bound ribosomes.**

Monitoring Editor
Judith Klumperman
University Medical Centre
Utrecht

Received: Dec 8, 2010
Revised: Apr 27, 2012
Accepted: May 3, 2012

INTRODUCTION

The endoplasmic reticulum (ER) is composed of a network of "rough," ribosome-studded sheets and smooth tubules that are continuous with the nuclear envelope. These subdomains are plastic and are remodeled in response to the needs of the cell. During interphase, enhanced protein synthesis and secretion promote morphology rich in sheets and rough ER (Wiest *et al.*, 1990; Benyamini *et al.*, 2009; Ueno *et al.*, 2010), whereas lipid and steroid synthesis and detoxification promote abundant tubular smooth ER (Black *et al.*, 2005). In adherent cultured cells, the ER is often described as having a network organization such that sheets are found close to, and tubular networks farther away from, the nucleus (Terasaki *et al.*, 1986; Puhka *et al.*, 2007). Mitotic ER reorganization has been analyzed in a number of studies, and great variation was reported both in the location and density of the mitotic ER in different cell types (Terasaki, 2000; Bobinnec *et al.*, 2003; McCullough and Lucocq, 2005; Poteryaev *et al.*, 2005). However, the exact structural changes in the ER have been only rarely addressed, possibly owing to difficulties in resolving the ER in the *z*-axis of light microscopy (LM) and to limited possibilities for doing three-dimensional (3D) analysis at the electron microscopy (EM) level with sufficient volumes.

We previously characterized the transformation of ER sheets to tubules during mitosis in CHO-K1 cells and showed that this transformation is accompanied by a reduction in membrane-bound ribosomes (Puhka *et al.*, 2007). These results suggest a sheet-stabilizing role for ribosomes or polysomes that are connected via translocon complexes to the luminal polypeptide folding and modification machinery. This idea is supported by a recent study in which sheet-forming proteins were proposed to associate with and be concentrated by polysomes (Shibata *et al.*, 2010). ER membrane–bound microtubules may stabilize rough ER by physically limiting the lateral mobility of polysomes (Nikonov *et al.*, 2002, 2007). The two most interesting microtubule-binding proteins in this respect are p180, which also binds ribosomes to create a platform for high-rate protein synthesis (Ogawa-Goto et al., 2007; Benyamini *et al.*, 2009; Ueno *et al.*, 2010), and CLIMP-63, whose ability to oligomerize may facilitate creation of a flat-sheet morphology (Klopfenstein *et al.*, 2001; Shibata *et al.*, 2010). The consensus is that ribosomes are more enriched in sheets than in tubules, and it has been suggested

This article was published online ahead of print in MBoC in Press (http://www.molbiolcell.org/cgi/doi/10.1091/mbc.E10-12-0950) on May 9, 2012.

*These authors are students of the Viikki Graduate School in Molecular Biosciences, University of Helsinki, Helsinki, Finland.

Address correspondence to: Eija Jokitalo (Eija.Jokitalo@Helsinki.fi).

Abbreviations used: EM, electron microscopy; ER, endoplasmic reticulum; ET, electron tomography; FS, freeze substitution; HPF, high-pressure freezing; HRP, horseradish peroxidase; LM, light microscopy; PM, plasma membrane; SBF-SEM, serial block-face scanning EM; ss, signal sequence; TEM, transmission EM; wt, wild type.

that polysomes may in fact not be physically compatible with high-curvature membranes (Shibata *et al.*, 2006). However, proteins associated with the nascent polypeptide translocation channel are found in smooth ER (Black *et al.*, 2005), and references to "rough ER tubules" occur frequently in the literature. Furthermore, high-curvature membranes are not exclusive to tubules but can also be found, for example, on the edges of ER sheets (Kiseleva *et al.*, 2007; Shibata *et al.*, 2010; Sparkes *et al.*, 2010). In the absence of proper quantification of ribosomes with respect to specific ER structures, however, the segregation of the rough ER and smooth ER domains remains descriptive and often obscure.

In addition to sheets and tubules, the third form of ER is fenestrated ER sheets, which were described originally by Palade (1956). Later, they were detected in a wide range of species and cell types (Lieberman, 1971; Orci *et al.*, 1971, 1972; Waugh *et al.*, 1973; Tani *et al.*, 1975; Brown, 1978; Hepler, 1981; Hepler *et al.*, 1990; Novikoff *et al.*, 1983; Rambourg *et al.*, 2001; West *et al.*, 2011), indicating that the ER has an intrinsic capacity to form fenestrations. Apart from this information, however, virtually nothing is known about the fenestrated sheets—for example, how do their dynamics, biogenesis, or even structure relate to those of intact sheets and tubules? The fenestrated sheets could be envisioned either as permanent structures or as intermediates in the transformation from sheets to tubules that occurs, for example, during mitosis in CHO-K1 cells (Puhka *et al.*, 2007).

Our work with CHO-K1 cells (Puhka *et al.*, 2007) was recently criticized by Lu *et al.* (2009, 2011), who argued that transformation of CHO-K1 ER sheets to tubules during mitosis and ER fenestration is a consequence of aldehyde fixation. They suggested an opposing model in which most of the ER is organized as extended cisternae in mitotic cells, with a very small fraction remaining organized as tubules. To address this issue, we analyzed both the detailed structural changes and reorganization of the ER during mitosis in several mammalian cell types at high resolution with transmission EM (TEM), electron tomography (ET), and serial block-face imaging using scanning EM (SBF-SEM), using both chemical fixation and high-pressure freezing (HPF) methods. SBF-SEM allows the imaging of whole cells at a resolution sufficient to easily identify 60-nm vesicles and slightly larger ER fenestrations (Denk and Horstmann, 2004; Zankel *et al.*, 2009). The results were correlated with diffraction-limited LM. We quantified the density of ER membrane–bound ribosomes in different ER structures: intact or fenestrated sheets, sheet edges, fenestrations, and tubules. From our data it is evident that the ER has several morphological features that are beyond the resolution of conventional LM. We suggest that the discrepancy between our previous results and those of the Kirchhausen group is due to the misinterpretation that ER network reorganization reflects an actual structural change in the ER (Lu *et al.*, 2009); such a misinterpretation may arise when ER structures are analyzed primarily at the LM level.

RESULTS

The ER in mitotic CHO-K1 cells is mainly tubular

We previously characterized the transformation of ER sheets to a tubular network in mitotic CHO-K1 cells using live-cell imaging, TEM, and ET of chemically fixed and cytochemically stained samples (Puhka *et al.*, 2007). Recently, however, Lu *et al.* (2009) presented an opposing view that the tubulation was a result of chemical fixation and that cells in general had a cisternal ER organization during mitosis. It is notable that although Lu *et al.* (2009) claimed that they used the same cell line, they did not present any data using CHO-K1 cells. CHO-K1 and CHO cells have different DNA content (Kao and Puck, 1968) and thus should be regarded as separate cell lines. Therefore, to correctly evaluate the impact of chemical fixation versus HPF on mitotic ER morphology, we prepared new samples of CHO-K1 cells using HPF and freeze substitution (FS) for 3D analysis using ET. This cell line was one of those used in our previous studies (Puhka *et al.*, 2007) and stably expressed green fluorescent protein tagged with a signal sequence (ss) and the tetrapeptide KDEL, which serves as an ER retention signal. The ER in the ET model spanning five 250-nm-thick sections of a metaphase CHO-K1 cell was predominantly tubular and lacked sheets (Figure 1; ET model in Supplemental Video S1). The main difference from our previous, chemically fixed sample was that the organelles appeared more rounded or smooth, indicating that HPF/FS material is more resistant to potential artifacts produced by dehydration and embedding. From this, we concluded that chemical fixation does not create fenestration or tubulation of ER membranes in mitotic CHO-K1 cells and that ER in these cells undergoes almost complete transformation from sheets to tubules during mitosis.

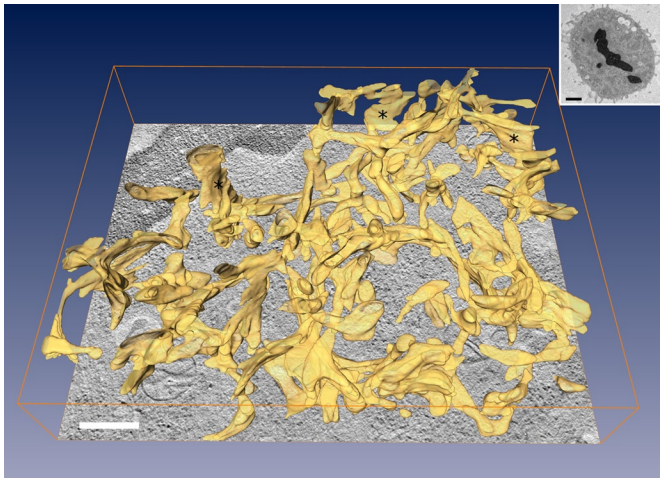

FIGURE 1: 3D model of the ER, showing a tubular network in a metaphase CHO-K1 cell prepared using HPF/FS. The ER model was derived from five 250-nm sections. Tubules are clearly the predominant morphology, and the nominal persisting sheets (*) are very small. Bars are 0.5 µm in the tomogram and 2 µm in the inset, which shows an overall view of the cell.

Interphase ER network organization and sheet morphology vary among cell types

Before any general conclusions about the structural transformation of ER during mitosis could be made, a good understanding of ER structures in several cell lines of different origins was needed. In our previous study, we analyzed only CHO-K1 cells (Puhka *et al.*, 2007), and thus we started by observing the ER during interphase in four commonly used epithelial cell lines—Huh-7, NRK-52E, HeLa, and Vero cells—by live-cell imaging. Of these, HeLa is the oldest and most commonly used cell line, and the other three are kidney and liver cells of human, rat, or African green monkey origin and were chosen because they are professional secretory cells with abundant ER. The cells expressed ssGFP-KDEL or Hsp47-GFP as a marker for the ER (Figure 2 and Supplemental Figure S1; Puhka *et al.*, 2007). During interphase, many mammalian cell lines have more ER sheets close to the nucleus compared with peripheral regions, where tubular networks prevail (Terasaki *et al.*, 1986; Puhka *et al.*, 2007). This organization was observed in interphase Vero and HeLa cells (Supplemental Figure S1, A and B). In contrast, interphase Huh-7 and NRK-52E cells diverged from the typical pattern and had a very large number of sheets that often extended to the cell periphery

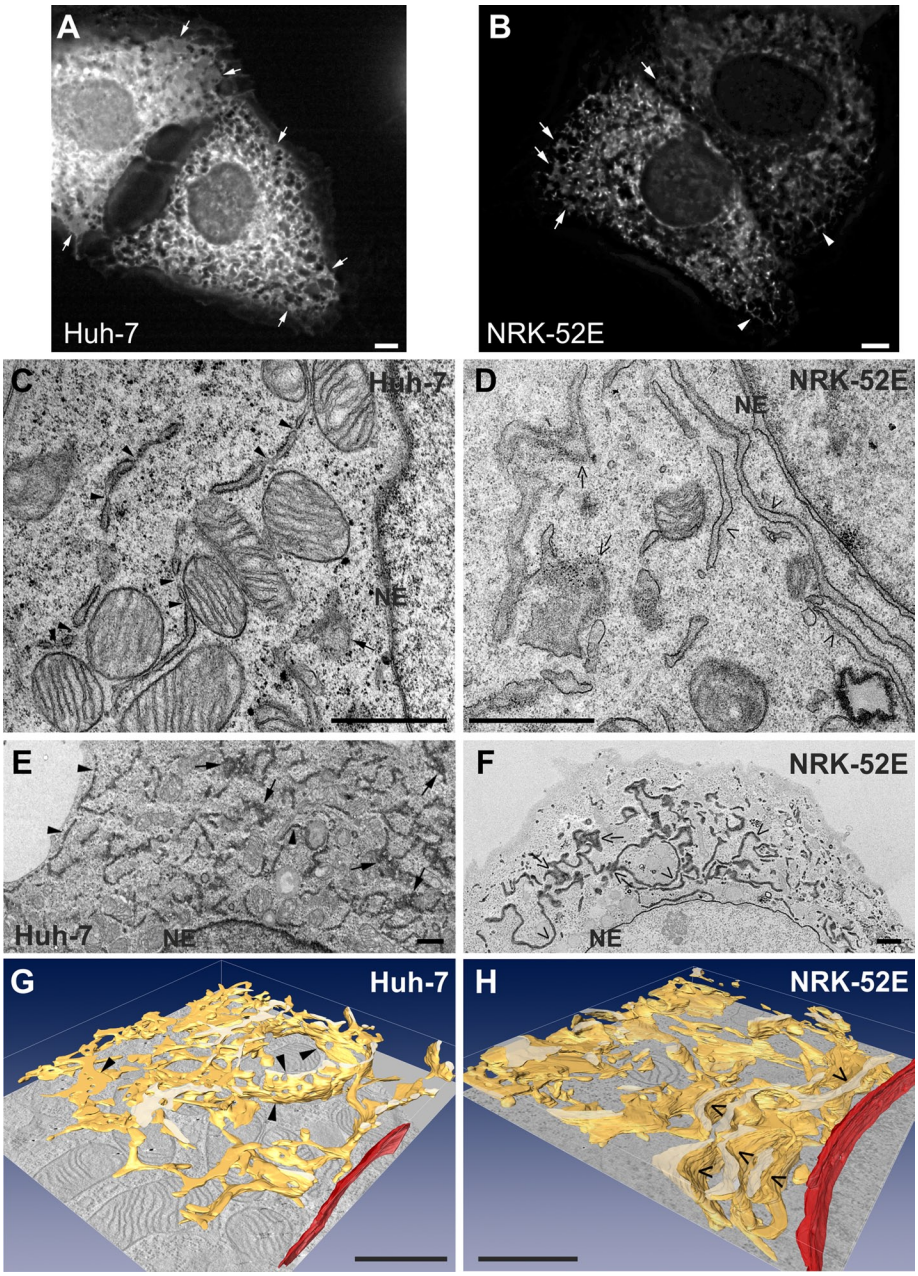

FIGURE 2: Interphase ER in Huh-7 and NRK-52E cells consists mainly of sheets; however, sheet profiles in thin sections of interphase Huh-7 cells are segmented and fenestrated as compared with NRK-52E. Huh-7 and NRK-52E cells expressing Hsp47-GFP were subjected to wide-field microscopy. Huh-7 cells have abundant peripheral sheets (arrows), as shown in A. NRK-52E cells (B) also have many sheets (arrows) and small areas of tubular networks (arrowheads) in the cell periphery. In EM micrographs, transverse sections of sheets in wt (C) and cytochemically stained (E) Huh-7 cells show multiple gaps (arrowheads), and many fenestrations are exposed in longitudinal sections of sheets (arrows). In contrast, transverse sections reveal long sheet profiles (open arrowheads) in NRK-52E cells, and longitudinal sections (open arrows) show sheets that are often completely intact in wt (D) and cytochemically stained (F) cells. ET analysis of the ER in Huh-7 and NRK-52E interphase cells clearly show the fenestrated nature of the ER sheets in Huh-7 cells (G, arrowheads) as compared with the intact sheets in NRK-52E cells (H, open arrowheads). The samples for ET were prepared by HPF/FS. The modeled volumes are derived from two 250-nm-thick sections. NE, nuclear envelope. Bars, 5 μm (A, B), and 1 μm (C–H).

(Figure 2, A and B). Tubules were interconnected with sheets and only rarely formed extensive tubular networks.

To study the ER in detail, we prepared chemically fixed samples with or without cytochemical staining of the ER, as well as HPF/FS samples, and analyzed them with conventional thin-section TEM and ET. For cytochemical staining of the ER, cells were transfected to transiently express ss horseradish peroxidase (HRP)–KDEL (Puhka *et al.*, 2007). The abundant sheet structures in Huh-7 cells (Figure 2, C and E) contained numerous fenestrations that appeared as sites of constriction or small gaps in transversely sectioned sheets and as roundish holes in longitudinally sectioned sheets. Fenestrations of similar size or quantity were not found in NRK-52E sheets (Figure 2, D and F), where transverse sections of sheets were long and without gaps, and longitudinal sections revealed no fenestrations in the majority of sheets. The same morphological features were evident by ET analysis of specimens that were subjected to HPF/FS, where fenestrations in Huh-7 sheets (Figure 2G and Supplemental Video S2) and more intact sheets in NRK-52E cells (Figure 2H and Supplemental Video S3) could be directly visualized. Thin-section EM analysis of chemically fixed wild-type (wt) Vero and HeLa cells (Supplemental Figure S1, C and D) showed ER sheets that had more fenestrations than NRK-52E cells, albeit significantly less than Huh-7 cells.

The fenestrations in Huh-7 cells did not appear to have a specific pore structure; that is, they varied somewhat in shape and size, averaging 75 ± 3 nm in diameter (n = 39 structures). Fenestrations were found irrespective of fixation method used and in both wt cells and cells expressing ER marker proteins. Moreover, the fenestrations were not abolished when cells were exposed to various ER stressors, including treatment with thapsigargin (to inhibit sarco/endoplasmic reticulum Ca^{2+}-ATPase pump function), increase of the pH to 9.0 or decrease to it 5.0, treatment with latrunculin A or nocodazole (to depolymerize actin or dynamic microtubule cytoskeleton, respectively), or deprivation of serum (to perturb lipid metabolism). Thus the fenestrations seem to be remarkably stable structures. Together these results clearly indicated that different cell types show large variations in the proportions of sheets and tubules, as well as in the morphology of the sheets themselves.

Mitotic ER network can be reorganized into concentric layers

Next we characterized the mitotic ER of these cell types by LM, TEM, and two different 3D-EM imaging techniques, namely ET and SBF-SEM. By LM, we found that the mitotic ER was aligned along the plasma membrane (PM) in concentric layers in Huh-7, Vero, and HeLa cells, a feature that was not found in CHO-K1 cells (Puhka *et al.*, 2007). However, this was not the exclusive organization

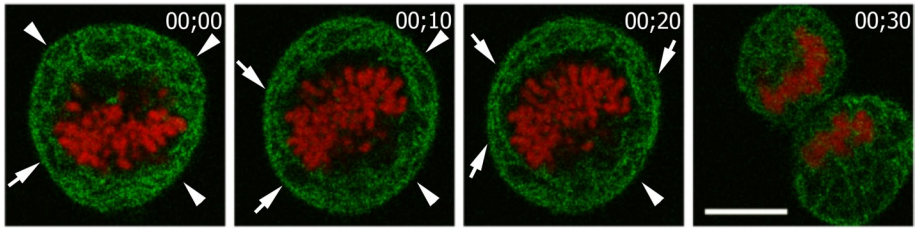

FIGURE 3: The reorganization of ER into concentric layers seems to be more predominant toward the end of metaphase. Huh-7 cells were cotransfected with pHsp47-GFP and pH2B-monomeric red fluorescent protein and imaged by confocal microscopy at 10-min intervals starting from early metaphase (time 00:00) and progressing through telophase. A deconvoluted optical section of consecutive time points demonstrates the progressive reorganization of ER from the reticular appearance at early metaphase (arrowheads) toward concentric layers at the end of metaphase (00:20, arrows). Bar, 10 μm.

in any of the cell lines we analyzed, and it was common to find cells or regions of cells where the mitotic ER appeared mainly reticular. This reorganization of the ER into concentric layers seemed to be more predominant toward the end of metaphase, as shown in Figure 3, where the same Huh-7 cell was imaged in 10-min intervals starting from early metaphase and progressing to telophase. In addition, LM and EM analysis showed that the appearance of ER layers seemed to coincide with the rounding of the cells during mitosis. To study the mitotic organization of ER in detail, we used SBF-SEM to image an early-metaphase Huh-7 cell that was still in the process of rounding up (Supplemental Figure S2 and Supplemental Video S4). The data set of the whole mitotic cell consists of 201 serial block-face images in 50-nm intervals covering a total volume of 6480 μm^3 (24 × 27 × 10 μm). From this cell, we modeled two regions of ER from opposite sides of the cell (Supplemental Figure S2, C and D). On the flatter side of the cell, the ER had a predominantly spread network organization, whereas on the more rounded side the ER was packed into concentric layers.

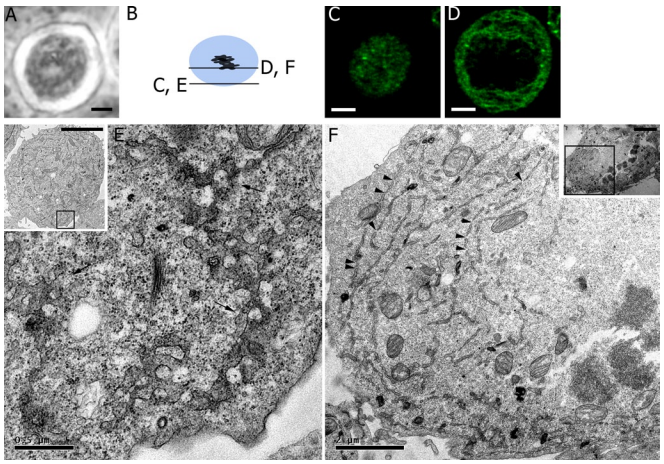

FIGURE 4: Correlative-light EM of a metaphase Huh-7 cell. A Huh-7 cell transiently coexpressing ssGFP-KDEL and ssHRP-KDEL was cultured on a glass-bottom dish (A, phase contrast image) and imaged by confocal microscopy (C, D) before chemical fixation and cytochemical staining for EM (E, F). (C) An optical section from the adhering side of the cell (see illustration in B) shows sheet profiles and some ER network. Highly fenestrated ER sheet profiles (arrows) are found in a thin-section EM image (E) from the same height (derived from the boxed region in inset). (D) An optical section from the middle of the cell shows multiple layers of long ER profiles coaligned with the PM. (F) The corresponding thin-section image (from the boxed region in inset) shows similar but gapped ER profiles (arrowheads). Thick sections for ET were cut in between the thin sections (E, F), and the tomogram is provided in Supplemental Video S4. Bars, 5 μm (A, C, D, and insets of E and F), 0.5 μm (E), and 2 μm (F).

The extent of mitotic sheet-to-tubule transformation varies among cell types and includes an intermediate phenotype of fenestrated sheets

To directly compare mitotic ER structures acquired by LM and EM, we performed correlative-light EM including ET analysis of Huh-7 cells coexpressing ssGFP-KDEL and ssHRP-KDEL (metaphase cell in Figure 4; tomogram in Supplemental Video S5). The concentric layers of long ER profiles observed at the LM level could be resolved by EM, revealing largely fenestrated sheets. Their alignment parallel to the PM was more evident in sections obtained from the middle of the cell (Figure 4, D and F). Sections from the adhering side of the cell, where ER was mostly parallel to the sectioning plane, showed large profiles of sheets with extensive fenestrations (Figure 4E). In some areas, the fenestrated sheets were very difficult to distinguish from tight planar tubular networks. These results suggested that fenestrations are not resolvable with diffraction-limited LM, as demonstrated directly by correlative-light EM.

To study mitotic ER morphology further, we imaged six additional prometaphase-to-metaphase Huh-7 cells using the SBF-SEM technique. The data set for one metaphase cell consisted of 412 serial block-face images at 50-nm intervals, covering a total volume of 11,025 μm^3 (21 × 21 × 25 μm; Figure 5 and Supplemental Video 6, A and B). In the complete 3D model, the dense arrangement of the ER made it difficult to discern structural details. Therefore here we show only a part of the model, which revealed numerous fenestrated sheets and short tubules forming concentric ER layers in the cell cortex (Figure 5, A–D). Sheets were smaller or more fenestrated compared with interphase ER. The side-view image revealed that many of the sheets are so heavily fenestrated that they resemble more of a tubular network (Figure 5C). Instead of forming an extensive 3D network, however, these tubules tended to remain organized in planar layers together with the fenestrated sheets. In addition, modeling the middle parts of the cell revealed the existence of numerous long tubules originating from the cortical ER layers and extending toward the mitotic spindle and the center of the cell (Figure 5, D and E).

LM imaging of mitotic NRK-52E cells suggested that ER sheets are retained at least to some extent during mitosis (Figure 6A). Analysis of thin EM sections of chemically fixed wt cells (unpublished data) or cytochemically stained cells expressing ssHRP-KDEL showed profiles of heavily fenestrated sheets in addition to tubular profiles (Figure 6B). TEM imaging of HPF/FS samples verified the results obtained with chemical fixation. In addition, we made tomographic series of two metaphase NRK-52E cells prepared by HPF/FS. The model in Figure 6C (animated model in Supplemental Video S7) shows fenestrated sheets intermixed with short tubules that tended to remain in planar layers. However, some regions had greater tridimensionality and appeared more reticular. Thin-section TEM images of mitotic Vero and HeLa cells were reminiscent of Huh-7 and NRK-52E cells and showed extensively fenestrated ER sheets along with tubular profiles (Supplemental Figure S3, C and D).

The observed rearrangement of the ER was quantified by measuring ER profile lengths in TEM images from thin sections of

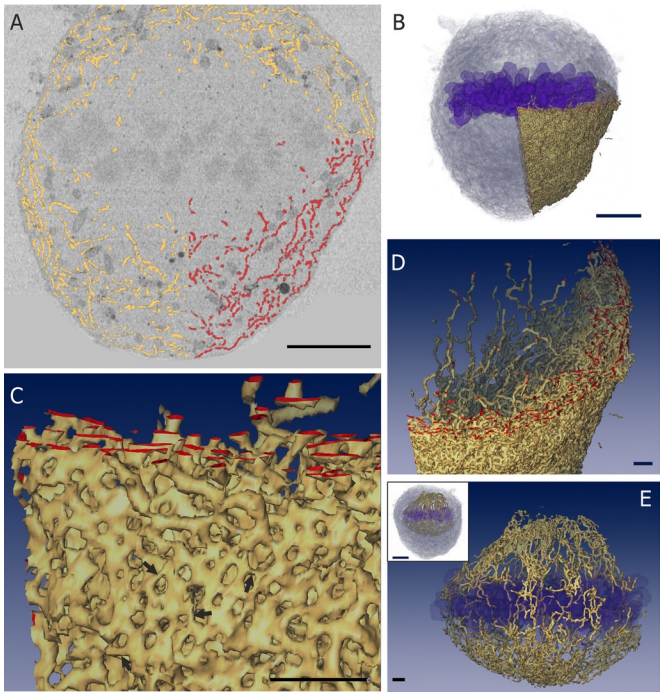

FIGURE 5: Model of a metaphase Huh-7 cell imaged with the SBF-SEM technique. A whole Huh-7 cell transiently expressing ssHRP-KDEL was chemically fixed, cytochemically stained, and imaged with SBF-SEM (Supplemental Video S6A), providing a voxel size of 27 × 27 × 50 nm, and the ER was modeled. (A) An image of one block-face overlaid with the modeled ER. For a clear view, a small part of the cell and ER model (A–D, Supplemental Video S6B) is shown starting from the metaphase plate of the chromosomes (A, B), including the spindle region (A, D) and the cortical parts (B, C). Cutting surface is marked with red color. Organization of the ER in cortical layers is visible in the block-face image (A) and views of the 3D model (C, D). The cortical layers are composed of fenestrated sheets and short tubules (C; tubules are marked with arrows). Long tubules originating from the cortical ER extend toward the middle of the cell (D, E). A view covering the complete middle part of the cell shows that this tubular part is quite extensive (E). Bars, 5 μm (A, B, and inset of E) and 1 μm (C–E).

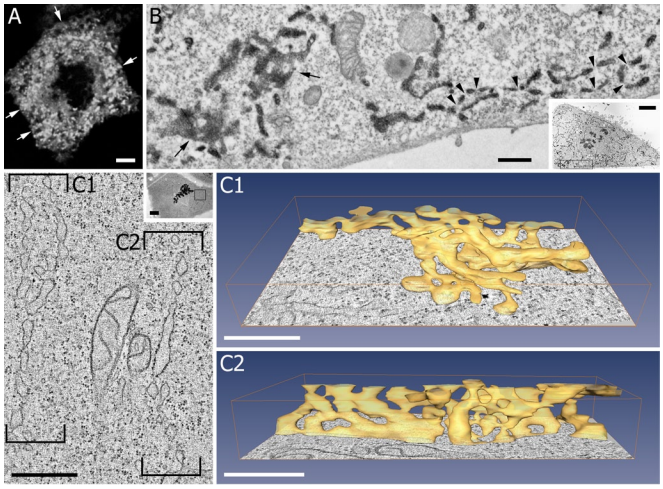

FIGURE 6: NRK-52E cells show fenestrated ER sheets and tubules during mitosis. The flat shape of a metaphase NRK-52E cell helps to expose many ER sheets in a confocal optical section (arrows in A). (B) A thin-section image of cytochemically stained ER in a metaphase NRK-52E cell shows longitudinal profiles of sheets with perforations (arrows) and long lines of transverse sheet profiles with multiple gaps (arrowheads) parallel to the PM. Cells transiently expressed Hsp47-GFP in A and ssHRP-KDEL in B as ER markers. (C) Two successive 250-nm sections of a wt metaphase NRK-52E cell prepared using HPF/FS were subjected to ET (also see Supplemental Video S7). Models of two neighboring ER structures (marked in the tomographic slice as C1 and C2) are composed of extensively fenestrated sheets, and tubules and are shown separately to allow easier visualization. Bars, 5 μm (A and insets of B and C) and 0.5 μm (the rest).

interphase and mitotic Huh-7 and NRK-52E cells (Figure 7). For the analysis, wt cells were detached from the culture dish after fixation and embedded as a pellet to ensure random orientation of cells and ER profiles on thin sections. As the cells were not synchronized in any way, the mitotic Huh-7 cells consisted of a natural representation of various ER network organizations; uniform networks were prevalent in 13% of cells, concentric ER layers were prevalent in 57%, and the remaining 30% of cells had both features (n = 23 prometaphase-to-anaphase cells). This analysis revealed that the fraction of short ER profiles (0–249 and 250–499 nm) increased by >70% during mitosis in both cell types ($p < 0.01$), just as in CHO-K1 cells (Puhka *et al.*, 2007). In addition, the longest profiles were <1500 nm long in mitotic cells but exceeded 2000 nm during interphase. The point of divergence was ~1000 nm; below this point, mitotic cells had more profiles than interphase cells, and the reverse was true above this point. Indeed, for profiles >1000 nm, the reduction between interphase and mitotic cells was >70% in both cell types (75% in NRK-52E and 79% in Huh-7; $p < 0.05$).

Together these findings suggested that fenestrated sheets are a common ER structure in interphase Huh-7 cells and in many mammalian cell types during mitosis. Along with tubules, they account for the observed increase in short ER profiles during mitosis. The spatial organization of the ER and the extent of mitotic sheet-to-tubule transformation vary among different cells but clearly exist. Thus diffraction-limited LM should not be used to resolve ER morphology but rather to assess the ER distribution within the cell. Reorganization of ER into concentric layers and structural changes of ER sheets during mitosis are two separate events that occur in parallel in certain cell types. Our morphometric analysis indicated that ER profiles get shorter even in cells in which ER is packed into concentric layers.

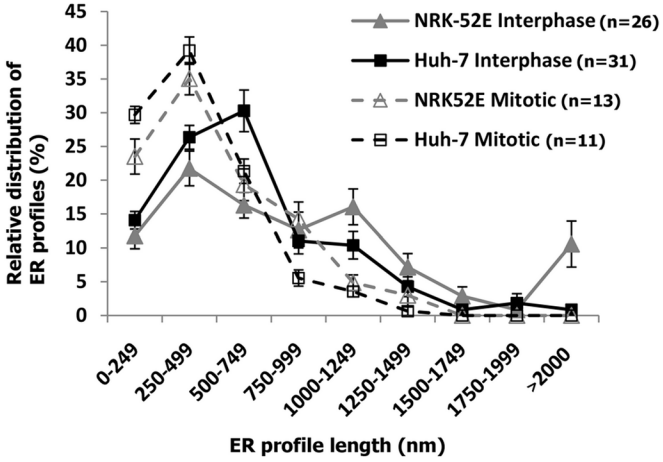

FIGURE 7: Relative distribution of thin-section ER profiles by length category demonstrates that mitotic Huh-7 and NRK-52E cells have more short profiles and fewer long profiles than their respective interphase cells. Similar, albeit smaller, differences are observed between Huh-7 and NRK-52E interphase cells. Error bars indicate ± SEM. Numbers (n) in the image refer to the number of cells analyzed.

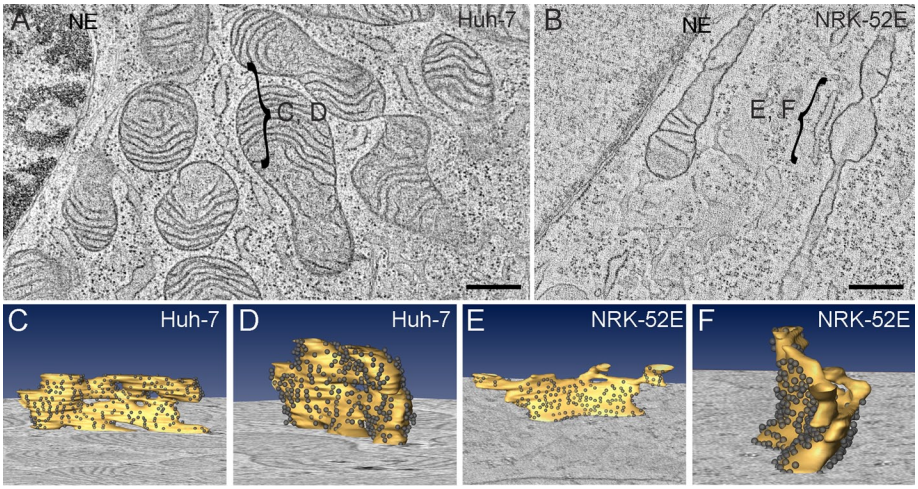

FIGURE 8: Modeling of ER and ribosomes from tomograms. Samples of Huh-7 (A, C, D) and NRK-52E (B, E, F) cells were prepared by HPF/FS, and individual sheets with ribosomes were modeled from the resulting tomograms. An example of a fenestrated sheet of the Huh-7 cells and a more intact sheet in NRK-52E cells are marked with a right bracket (}) in the tomogram slice. The corresponding models show that highly curved membranes (sheet edges in D and E, fenestrations in C, and tubules in E) tend to have fewer ribosomes. Bars, 0.5 µm (A, B).

Ribosome density correlates inversely with increased fenestration of sheets and tubulation

We previously showed that the ER in CHO-K1 cells undergoes sheet-to-tubule transformation upon dissociation of ER-bound ribosomes (Puhka *et al.*, 2007). In CHO-K1 cells, in which the sheet-to-tubule transition was nearly quantitative, there was a 70% decrease in the amount of ER-bound ribosomes between interphase and metaphase profiles (Puhka *et al.*, 2007). Given that Huh-7 and NRK-52E cells showed cisternal retention and lesser sheet-to-tubule transition during mitosis, we measured ribosome density of interphase and mitotic ER in Huh-7 and NRK-52E cells. Random thin-section TEM images were acquired from chemically fixed cells, and ribosomes were individually counted from transversely sectioned ER membranes (as described in Puhka *et al.*, 2007). The mean number of ribosomes/µm in interphase was 17.3 ± 1.2 (n = 22 cells, total of 1403 ribosomes counted per 80.0 µm of ER membrane) for NRK-52E cells and 15.1 ± 0.7 (n = 24 cells, 1422 ribosomes per 87.6 µm) for Huh-7 cells. During mitosis, these respective numbers decreased to 9.8 ± 0.5 ribosomes/µm^2 (43% decrease; n = 10 cells, 3293 ribosomes/328.5 µm) and 8.3 ± 0.4 ribosomes/µm (45% decrease; n = 12 cells, 3052 ribosomes/397 µm; $p < 0.001$ for both).

To assess the density of ER-bound ribosomes on intact sheets, fenestrated sheets, and tubules of interphase cells, we prepared Huh-7 and NRK-52E samples using HPF/FS and quantified ribosomes from thin-section TEM images. In NRK-52E cells, the transverse sections of intact sheets contained the highest ribosome density: 24.6 ± 0.9 (SEM) ribosomes/µm (n = 35 structures). In comparison, the fenestrated sheets of Huh-7 cells had 19.8 ± 1.1 (SEM) ribosomes/µm (n = 41 structures; 20% difference, $p < 0.01$). On sheet edges and fenestrations, the ribosome density was even lower: 16.9 ± 1.1 (SEM) ribosomes/µm in NRK-52E (n = 64 structures) and 15.4 ± 1.0 (SEM) ribosomes/µm in Huh-7 (n = 68 structures); these values were >30% lower compared with transverse sections of intact sheets ($p < 0.001$). Round profiles and tubular side views (i.e., tubular membranes) clearly contained the lowest ribosome density in both cell types, 4.9 ± 0.6 (SEM) ribosomes/µm (n = 80 structures) in NRK-52E cells and 8.2 ± 0.8 (SEM) ribosomes/µm (n = 80 structures) in Huh-7 cells; these values were >60% lower compared with transverse sections of intact sheets ($p < 0.001$). The structures in the foregoing categories were derived from 15–28 cells per cell type.

Because there is always some uncertainty when identifying ER structures in thin sections, we also quantified ribosomes per membrane surface area in HPF/FS tomograms (Figure 8). Each structure was modeled separately, and the parts connected to other structures were left out to obtain a good estimate of ribosome number purely in the desired category. Intact sheets from an NRK-52E tomogram (n = 4 sheets) had 824 ± 57 ribosomes/µm^2, whereas a somewhat lower value of 786 ± 69 ribosomes/µm^2 was obtained for fenestrated sheets in Huh-7 cells (n = 5 sheets). Tubules clearly had fewer ribosomes in both cell types: 203 ± 26 ribosomes/µm^2 for NRK-52E (n = 8 tubules) and 137 ± 20 ribosomes/µm^2 for Huh-7 (n = 9 tubules). The lower density of ribosomes on fenestrations, edges of sheets, and tubules was visible in the ET models (Figure 8, C–F). In conclusion, ribosome density correlates inversely with the amount of tubules and fenestration of sheets. Together the findings support the idea that high-curvature surfaces tend to have a low density of ribosomes and perhaps polysomes.

DISCUSSION

We previously reported that the ER undergoes a sheet-to-tubule transition during mitosis in cultured CHO-K1 cells (Puhka *et al.*, 2007). The Kirchhausen group (Lu *et al.*, 2009) published a paper in which they claimed the opposite. To address the discrepancy, we have now shown that transition of sheets to tubules in CHO-K1 cells is indeed not a result of chemical fixation artifacts, because we obtained similar results using HPF/FS. Chemical fixation has been used in most high-resolution morphology studies, and these results form the basis for our present view of the structure of the ER and other organelles. Murk *et al.* (2003) compared chemical and cryofixation methods and demonstrated that chemical fixation resulted in some shrinkage and deformation of early and late endosomes but did not alter the structure of lysosomes in the same cell. We also agree that HPF/FS is a superior technique for preserving the fine ultrastructure of organelles and consider HPF/FS as the method of choice for high-resolution structural studies using ET. As with every method, however, HPF/FS has its limitations—it requires special equipment and expertise and must be optimized for substitution protocols; moreover, the areas that undergo sufficient freezing and have good membrane contrast are usually quite small, especially on the ER. Here we analyze chemically fixed and HPF/FS-prepared cells side by side and conclude that, although the ER appears to be smoother after HPF/FS, chemical fixation does not substantially alter ER structure.

The Kirchhausen group observed that several cell lines have a tendency to reorganize their ER into concentric layers underneath the PM in mitotic cells. During our work with CHO-K1 cells, we imaged >200 naturally mitotic cells and did not encounter any that had the ER network clearly organized in this way. After analyzing several other cell lines, however, our results partially agree with those of Lu *et al.* (2009), showing a trend toward cisternal retention and concentric layer formation during mitosis in some cell lines. The tendency to pack ER in concentric layers during mitosis is likely a consequence

of many factors. McCullough and Lucocq (2005) suggested that the cortical association and layering of ER cisternae are dependent on the actin cytoskeleton and ER abundance, respectively. Our data imply that the layering correlates with cell rounding, the abundance of ER in cells, and the expression level of the marker proteins. Lu *et al.* (2009) used Lipofectamine for transfections, and from their images it is apparent that the transfected genes were highly expressed. In addition, they mainly used membrane marker proteins (GFP-Sec61β, GFP-Rtn4HD, and LBR-GFP), and it has been documented that overexpression of membrane proteins can yield expansion and deformation of membrane structures (Ellenberg *et al.*, 1997; Snapp *et al.*, 2003; Ma *et al.*, 2007). To minimize the risk of artifacts, we used FuGENE HD and FuGENE 6 to transfect cells and soluble luminal ER markers that, when overexpressed, leak to the *cis*-Golgi.

Our quantitative morphological comparison and 3D EM analysis of Huh-7 and NRK-52E cells clearly demonstrate that the mitotic ER undergoes transformation from intact or large sheets toward more fenestrated or smaller sheets and tubules. This is further supported by thin-section TEM analysis of Vero and HeLa cells. Lu *et al.* (2009) presented LM data of many cell types but only a few tomograms and 3D models of individual sheets in mitotic BSC1 cells. In our view these tomograms contain fenestrated sheets (slice images show lines of ER profiles separated by small gaps) and tubules, although this point was not disclosed in the article. The resolution of conventional LM is not sufficient to resolve subtle morphological changes such as fenestrations on ER sheets or differences between planar tight tubular networks and fenestrated sheets. Interpretation of images becomes even more challenging in those mitotic cells in which ER is packed into tight layers. In addition, the layers mostly align along the *z*-axis of imaging, which has the poorest resolution. Therefore a systematic EM-level analysis with sufficient statistics and volumes is needed to support LM data. Thus we suggest that the conflicting results are mainly due to misinterpretation of ER reorganization to complete structural transformation of tubules to sheets and in addition due to the use of different cell lines, lack of morphological analysis of interphase cells, and a limited amount of structures modeled from tomograms.

Our finding that intact sheet morphology is linked to high ribosome density indicates that certain cell types retain more intact sheets and ER-bound ribosomes during mitosis than others. This might be explained by different mechanisms with which various cell types effect translation inhibition during mitosis. Two translation regulation points have been identified: at initiation (Fan and Penman, 1970; Le Breton *et al.*, 2005) and during elongation (Sivan *et al.*, 2007). For example, mitotic HeLa cells, which have fenestrated ER sheets (Mullins, 1984; Supplemental Figure S3), predominantly inhibit elongation and retain polysomes during mitosis, albeit in a less active state (Sivan *et al.*, 2007). On the other hand, regulation of translation mainly at initiation would lead to disassembly of polysomes and a more tubular ER morphology.

We present a model in which the mitotic conversion of an intact sheet to a tubular network proceeds through appearance and enlargement of fenestrations until the structure resembles a tubular network (Figure 9). The conversion would be caused—directly or indirectly—by the ongoing loss of membrane-bound ribosomes. The starting point (intact vs. fenestrated sheets) and ending point (smaller intact or fenestrated sheets vs. tubules) may vary in a manner that is specific to cell type and ribosome density. The resulting mitotic morphology could be seen as a mosaic built by membrane-bending proteins (Voeltz *et al.*, 2006; Kiseleva, 2007; Shibata *et al.*, 2010) and by the remaining polysomes, which may move more freely owing to the relocation of microtubules (Nikonov *et al.*, 2002, 2007). Of interest, knockdown of p180, a ribosome-binding ER protein, leads to a reduced ribosome density on ER membranes (Benyamini *et al.*, 2009) and, in our view, to profiles of fenestrated sheets on thin sections. The level of p180 is naturally reduced immediately before cell division.

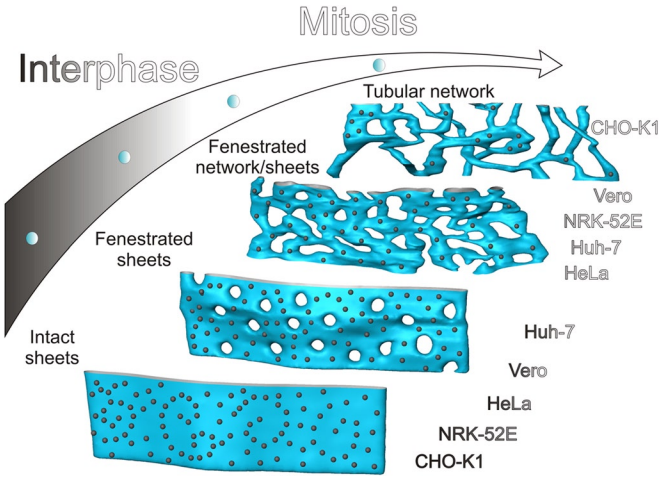

FIGURE 9: Model of mitotic sheet-to-tubule transformation. The transformation of rough ER starts from intact or fenestrated sheets and proceeds toward a more fenestrated state that can eventually produce structures resembling tubular networks. The extent of the shape change correlates with the density of membrane-bound ribosomes. The starting and ending points vary among cell types, but the direction of transformation remains the same in all cultured mammalian cells analyzed here. The arrow with the color gradient symbolizes the progression from interphase to metaphase. ER structures on the color scale and cell types are marked with dark colors in interphase and light colors during mitosis.

The dynamics, dimensions, and complicated network morphology of the ER make many of its substructures, such as fenestrations of the sheets, not resolvable by conventional LM. Because LM is required for visualization of ER dynamics and superresolution methods are still evolving, the best way to understand ER morphology is to combine LM and EM. In our hands, SBF-SEM analysis is a valuable asset for studying ER structures. SBF-SEM allows analysis of large volumes with sufficient resolution, and, if it is combined with cytochemical staining, the time spent in modeling becomes reasonable.

MATERIALS AND METHODS

Cell culture, transfection, constructs, and drug treatments

Huh-7 (JCRB0403; Japanese Collection of Research Bioresources Cell Bank, Osaka, Japan), Vero (CCL-81; American Type Culture Collection [ATCC], Manassas, VA), and HeLa (C3005-1; Clontech, Mountain View, CA) cells were cultured in EMEM containing 5 or 10% fetal bovine serum, 100 U/ml penicillin, 100 μg/ml streptomycin, and 2 mM L-glutamine (all from BioWhittaker, Lonza, Basel, Switzerland). Cell lines CHO-K1 (CCL-61; ATCC), CHO-K1/ssGFP-KDEL (Kuokkanen *et al.*, 2007), and NRK-52E (CRL-1571; ATCC) were cultured as described (Puhka *et al.*, 2007). All drugs used were from Sigma-Aldrich (St. Louis, MO). pH2B-mRFP (Keppler *et al.*, 2006) was obtained from the European *Saccharomyces cerevisiae* Archive for Functional Analysis (Institute for Molecular Biosciences, Johann Wolfgang Goethe-University Frankfurt, Frankfurt, Germany). Construction of pssGFP-KDEL is described in Kuokkanen *et al.* (2007). pssHRP-KDEL and pHsp47-GFP were provided by the respective laboratories of Connolly *et al.* (1994) and Kano *et al.* (2005). Cells were treated with 1–10 μM nocodazole for 10–30 min

to depolymerize dynamic microtubules (Friedmann *et al.*, 2010). Latrunculin A treatments were done at 1 µM concentration for 30–60 min, and thapsigargin treatments were at 100 nM for 2 h. Serum deprivation was done in normal cell culture medium without fetal bovine serum and with or without 2.5 mg/ml of lipoprotein-deficient serum (Chemicon, Temecula, CA) for 24 h. All transfections were done with FuGENE 6 or FuGENE HD (Roche, Indianapolis, IN) according to manufacturer's instructions. For cotransfections, a 1:1 (wt/wt) ratio of plasmids was used.

Light microscopy

All confocal images are from live cells and were acquired as described (Puhka *et al.*, 2007) with the following exceptions: we used a CO_2 supply or 15 mM 4-(2-hydroxyethyl)-1-piperazineethanesulfonic acid (HEPES) buffering, either unidirectional or bidirectional scanning over the range of 800–1400 Hz, line averaging of 2–4, and a *z*-step of 285–488 nm. Fixation and cytochemical staining for correlative-light EM were done immediately after acquiring the last image, as described (Jokitalo *et al.*, 2001). Wide-field images were acquired with AX70 Provis microscope using a Plan Apo 60×/1.40 or 100×/1.35 oil objective, an F-View II charge-coupled device (CCD) camera, and Image Analysis Software (Olympus, Tokyo, Japan) from fixed cells.

Electron microscopy

Cells for HPF were cultured on 1.5-mm-diameter sapphire disks for ≥1 d with or without a 50 µg/ml fibronectin coating (Sigma-Aldrich). Cells were overlaid with 20% BSA (Sigma-Aldrich) in DMEM (BioWhittaker) at 37°C and frozen on a gold specimen carrier using a Leica EM PACT High-Pressure Freezer (Leica, Wetzlar, Germany). FS was performed in a Leica EM AFS2 Automated FS unit using 2% OsO_4, 0.3% uranyl acetate, and 10% water in absolute ethanol and the following temperature ramp: –90°C for 10 h, –90 to –20°C over 7 h, and –20 to +4°C over 3 h. Samples were washed three times with cold acetone and then infiltrated with 1:1 acetone and Epon (TAAB, Aldermaston, United Kingdom) for 30 min, Epon alone for 30–45 min, and Epon again for >2 h. Polymerization was carried out at 60°C for >14 h. Sapphire disks were dissociated with a sharp edge tool (Leica) on a hot plate, and 60-nm sections were cut parallel to the block-face plane. Flat-embedded samples used for ribosome quantification and other EM samples were prepared as described (Jokitalo *et al.*, 2001; Puhka *et al.*, 2007), except that cells for pellet samples used in all quantifications were scraped after fixation, collected by centrifuging at 5000 × *g* for 5 min, osmicated, dehydrated in a graded ethanol series and acetone, and infiltrated gradually with Epon at room temperature using the same protocol as for HPF/FS samples. Quantifications were carried out as described (Puhka *et al.*, 2007), except that only 60-nm sections and wt cells were used, and images were acquired with a MultiScan 794 1K × 1K CCD camera (Gatan, Pleasanton, CA) with 9300× magnification for ribosomes and 4800× for ER profile lengths. ER profile lengths were measured in random cellular views, using one image per interphase cell at a random location, or three to nine images per mitotic cell uniformly covering the cell profile.

Electron tomography

ET was done essentially as described (Puhka *et al.*, 2007), except that the tilt series images between ±62° were acquired with an UltraScan 4000 CCD camera, 4K × 4K (Gatan). Tilt series were acquired at nominal magnification of 9600, 7800, and 5000×, providing a pixel size of 2.28, 2.84, and 4.40 nm, respectively. Ribosomes on tomograms were quantified by manually tagging the ribosomes on separately modeled ER structures using IMOD software (Kremer *et al.*, 1996), and surface areas were measured using the surface measurement tool in Amira (Visage Imaging, San Diego, CA).

SBF-SEM

Preparation of the Huh-7 metaphase cell sample in Figure 5 included cytochemical staining and uranyl acetate en block staining and was done as described (Jokitalo *et al.*, 2001; Puhka *et al.*, 2007). All the other specimens were prepared using a protocol modified from Deerinck *et al.* (2010). The cells were grown on coverslips, fixed, and cytochemically stained as described (Jokitalo *et al.*, 2001), and thereafter all washes were shortened to 1 min and thiocarbohydrazide incubation to 10 min, and the second osmium incubation was done with a 1% OsO_4 solution. After standard dehydration steps, samples were flat embedded in hand-made silicone holders filled with 100% Durcupan ACM resin (Fluka, Sigma-Aldrich), clamped between two objective glasses, and infiltrated for at least 2 h before polymerization.

Images were acquired with a FEG-SEM Quanta 250 (FEI, Hillsboro, OR), using a backscattered electron detector (Gatan). The mitotic Huh-7 cell in Figure 5 was imaged with 2-kV beam voltage, spot size 3, and 0.23-Torr pressure, and in Supplemental Figure S2 with 2.6-kV beam voltage, spot size 3, and 0.30-Torr pressure. The microscope was equipped with a microtome (3View; Gatan), which allowed serial imaging of block faces with increments of 50 nm. The images were first processed and segmented using Amira and Microscopy Image Browser, a self-developed program written under Matlab environment, and further rendered in Amira.

Definitions of ER profiles for ribosome quantification from HPF samples

ER profiles on 60-nm HPF/FS EM sections were divided into three categories. 1) Transverse sections of sheets were at least 800 nm long along their midline and maximally 150 nm wide. In Huh-7 cells, fenestrated sheets were included with a maximum gap of ~100 nm between individual sheet profiles, which had to be clearly aligned, and the sum of their lengths was at least 800 nm. 2) Longitudinal sheet profiles had a diameter of ≥150 nm and could include fenestrations. Fenestrations were defined as being closed from all sides, and only frontal views were accepted. 3) The tubules category included round and side-view profiles of tubules. Round ER profiles had a ratio between the largest diameter and the diameter perpendicular to it no larger than 1.5 and contained at least one ribosome. Tubular side-view profiles were connected to wider ER profiles with ribosomes and often started from a three-way junction.

Statistical analysis and image processing

Statistical analysis was done with PASW Statistics 17 software (SPSS, IBM, Armonk, NY) using a *t* test for normally distributed data and a Mann–Whitney U test for data that were not normally distributed. All LM figures were deconvoluted using AutoQuant Autodeblur software (Media Cybernetics, Bethesda, MD). Brightness and contrast were adjusted with Photoshop CS4 (Adobe, San Jose, CA).

ACKNOWLEDGMENTS

We thank Mervi Lindman for technical assistance with ET samples, the Light Microscopy Unit of the Institute of Biotechnology, University of Helsinki, for providing facilities, and Joel Mancuso at Gatan for providing the SBF-SEM data set of the metaphase Huh-7 cell in Figure 5. This work was funded by the Academy of Finland (Project No. 131650), Biocenter Finland, and the Emil Aaltonen Foundation.

REFERENCES

Benyamini P, Webster P, Meyer DI (2009). Knockdown of p180 eliminates the terminal differentiation of a secretory cell line. Mol Biol Cell 20, 732–744.

Black VH, Sanjay A, van Leyen K, Lauring B, Kreibich G (2005). Cholesterol and steroid synthesizing smooth endoplasmic reticulum of adrenocortical cells contains high levels of proteins associated with the translocation channel. Endocrinology 146, 4234–4249.

Bobinnec Y, Marcaillou C, Morin X, Debec A (2003). Dynamics of the endoplasmic reticulum during early development of *Drosophila melanogaster*. Cell Motil Cytoskeleton 54, 217–225.

Brown D (1978). Fenestrae in the rough endoplasmic reticulum of *Xenopus laevis* hepatocytes. Anat Rec 191, 103–110.

Connolly CN, Futter CE, Gibson A, Hopkins CR, Cutler DF (1994). Transport into and out of the Golgi complex studied by transfecting cells with cDNAs encoding horseradish peroxidase. J Cell Biol 127, 641–652.

Deerinck TJ, Bushong EA, Thor A, Ellisman MH (2010). NCMIR methods for 3D EM: a new protocol for preparation of biological specimens for serial block face scanning electron microscopy. Available at: http://ncmir.ucsd.edu/sbfsem-protocol.pdf.

Denk W, Horstmann H (2004). Serial block-face scanning electron microscopy to reconstruct three-dimensional tissue nanostructure. PLoS Biol 2, e329.

Ellenberg J, Siggia ED, Moreira JE, Smith CL, Presley JF, Worman HJ, Lippincott-Schwartz J (1997). Nuclear membrane dynamics and reassembly in living cells: targeting of an inner nuclear membrane protein in interphase and mitosis. J Cell Biol 138, 1193–1206.

Fan H, Penman S (1970). Regulation of protein synthesis in mammalian cells. II. Inhibition of protein synthesis at the level of initiation during mitosis. J Mol Biol 50, 655–670.

Friedmann JR, Webster BM, Mastronarde DN, Verhey KJ, Voeltz GK (2010). ER sliding dynamics and ER-mitochondrial contacts occur on acetylated microtubules. J Cell Biol 190, 363–375.

Hepler PK (1981). The structure of the endoplasmic reticulum revealed by osmium tetroxide-potassium ferricyanide staining. Eur J Cell Biol 26, 102–111.

Hepler PK, Palevitz BA, Lancelle SA, McCauley MM, Lichtscheidl I (1990). Cortical endoplasmic reticulum in plants. J Cell Sci 96, 355–373.

Jokitalo E, Cabrera-Poch N, Warren G, Shima DT (2001). Golgi clusters and vesicles mediate mitotic inheritance independently of the endoplasmic reticulum. J Cell Biol 154, 317–330.

Kano F, Kondo H, Yamamoto A, Kaneko Y, Uchiyama K, Hosokawa N, Nagata K, Murata M (2005). NSF/SNAPs and p97/p47/VCIP135 are sequentially required for cell cycle-dependent reformation of the ER network. Genes Cells 10, 989–999.

Kao FT, Puck TT (1968). Genetics of somatic mammalian cells, VII. Induction and isolation of nutritional mutants in Chinese hamster cells. Proc Natl Acad Sci USA 60, 1275–1281.

Keppler A, Arrivoli C, Sironi L, Ellenberg J (2006). Fluorophores for live cell imaging of AGT fusion proteins across the visible spectrum. Biotechniques 41, 167–175.

Kiseleva E, Morozova KN, Voeltz GK, Allen TD, Goldberg MW (2007). Reticulon 4a/NogoA locates to regions of high membrane curvature and may have a role in nuclear envelope growth. J Struct Biol 160, 224–235.

Klopfenstein DR, Klumperman J, Lustig A, Kammerer RA, Oorschot V, Hauri HP (2001). Subdomain-specific localization of CLIMP-63 (p63) in the endoplasmic reticulum is mediated by its luminal alpha-helical segment. J Cell Biol 153, 1287–1300.

Kremer JR, Mastronarde DN, McIntosh JR (1996). Computer visualization of three-dimensional image data using IMOD. J Struct Biol 116, 71–76.

Kuokkanen E, Smith W, Mäkinen M, Tuominen H, Puhka M, Jokitalo E, Duvet S, Berg T, Heikinheimo P (2007). Characterisation and subcellular localisation of human neutral class II α-mannosidase. Glycobiology 17, 1084–1093.

Le Breton M, Cormier P, Bellé R, Mulner-Lorillon O, Morales J (2005). Translational control during mitosis. Biochimie 87, 805–811.

Lieberman AR (1971). Microtubule-associated smooth endoplasmic reticulum in the frog's brain. Z Zellforsch Mikrosk Anat 116, 564–577.

Lu L, Ladinsky MS, Kirchhausen T (2009). Cisternal organization of the endoplasmic reticulum during mitosis. Mol Biol Cell 20, 3471–3480.

Lu L, Ladinsky MS, Kirchhausen T (2011). Formation of the postmitotic nuclear envelope from extended ER cisternae precedes nuclear pore assembly. J Cell Biol 194, 425–440.

Ma Y, Cai S, Lv Q, Jiang Q, Zhang Q, Sodmergen, Zhai Z, Zhang C (2007). Lamin B receptor plays a role in stimulating nuclear envelope production and targeting membrane vesicles to chromatin during nuclear envelope assembly through direct interaction with importin beta. J Cell Sci 120, 520–530.

McCullough S, Lucocq J (2005). Endoplasmic reticulum positioning and partitioning in mitotic HeLa cells. J Anat 206, 415–425.

Mullins JM (1984). Spindle-membrane associations in freeze fractured HeLa cells. Cell Biol Int Rep 8, 107–115.

Murk JL, Posthuma G, Koster AJ, Geuze HJ, Verkleij AJ, Kleijmeer MJ, Humbel BM (2003). Influence of aldehyde fixation on the morphology of endosomes and lysosomes: quantitative analysis and electron tomography. J Microsc 212, 81–90.

Nikonov AV, Hauri HP, Lauring B, Kreibich G (2007). Climp-63-mediated binding of microtubules to the ER affects the lateral mobility of translocon complexes. J Cell Sci 120, 2248–2258.

Nikonov AV, Snapp E, Lippincott-Schwartz J, Kreibich G (2002). Active translocon complexes labeled with GFP-Dad1 diffuse slowly as large polysome arrays in the endoplasmic reticulum. J Cell Biol 158, 497–506.

Novikoff AB, Spater HW, Quintana N (1983). Transepithelial endoplasmic reticulum in rat proximal convoluted tubule. J Histochem Cytochem 31, 656–661.

Ogawa-Goto K, Tanaka K, Ueno T, Tanaka K, Kurata T, Sata T, Irie S (2007). p180 is involved in the interaction between the endoplasmic reticulum and microtubules through a novel microtubule-binding and bundling domain. Mol Biol Cell 18, 3741–3751.

Orci L, Matter A, Rouiller C (1971). A comparative study of freeze-etch replicas and thin sections of rat liver. J Ultrastruct Res 35, 1–19.

Orci L, Perrelet A, Like AA (1972). Fenestrae in the rough endoplasmic reticulum of the exocrine pancreatic cells. J Cell Biol 55, 245–249.

Palade GE (1956). The endoplasmic reticulum. J Biophys Biochem Cytol 2, 85–98.

Poteryaev D, Squirrell JM, Campbell JM, White JG, Spang A (2005). Involvement of the actin cytoskeleton and homotypic membrane fusion in ER dynamics in *Caenorhabditis elegans*. Mol Biol Cell 16, 2139–2153.

Puhka M, Vihinen H, Joensuu M, Jokitalo E (2007). Endoplasmic reticulum remains continuous and undergoes sheet-to-tubule transformation during cell division in mammalian cells. J Cell Biol 179, 895–909.

Rambourg A, Jackson CL, Clermont Y (2001). Three dimensional configuration of the secretory pathway and segregation of secretion granules in the yeast *Saccharomyces cerevisiae*. J Cell Sci 114, 2231–2239.

Shibata Y, Shemesh T, Prinz WA, Palazzo AF, Kozlov MM, Rapoport TA (2010). Mechanisms determining the morphology of the peripheral ER. Cell 143, 774–788.

Shibata Y, Voeltz GK, Rapoport TA (2006). Rough sheets and smooth tubules. Cell 126, 435–439.

Sivan G, Kedersha N, Elroy-Stein O (2007). Ribosomal slowdown mediates translational arrest during cellular division. Mol Cell Biol 27, 6639–6646.

Snapp EL, Hegde RS, Francolini M, Lombardo F, Colombo S, Pedrazzini E, Borgese N, Lippincott-Schwartz J (2003). Formation of stacked ER cisternae by low affinity protein interactions. J Cell Biol 163, 257–269.

Sparkes I, Tolley N, Aller I, Svozil J, Osterrieder A, Botchway S, Mueller C, Frigerio L, Hawes C (2010). Five *Arabidopsis* reticulon isoforms share endoplasmic reticulum location, topology, and membrane-shaping properties. Plant Cell 22, 1333–1343.

Tani E, Ametani T, Nakano K, Nishiura M, Higashi N (1975). Fenestrae in Golgi and endoplasmic reticulum cisternae of human brain tumours. Acta Neuropathol 31, 13–19.

Terasaki M (2000). Dynamics of the endoplasmic reticulum and Golgi apparatus during early sea urchin development. Mol Biol Cell 11, 897–914.

Terasaki M, Chen LB, Fujiwara K (1986). Microtubules and the endoplasmic reticulum are highly interdependent structures. J Cell Biol 103, 1557–1568.

Ueno T, Tanaka K, Kaneko K, Taga Y, Sata T, Irie S, Hattori S, Ogawa-Goto K (2010). Enhancement of procollagen biosynthesis by p180 through augmented ribosome association on the endoplasmic reticulum in response to stimulated secretion. J Biol Chem 285, 29941–29950.

Voeltz GK, Prinz WA, Shibata Y, Ris JM, Rapoport TA (2006). A class of membrane proteins shaping the tubular endoplasmic reticulum. Cell 124, 573–586.

Waugh RA, Spray TL, Sommer JR (1973). Fenestrations of sarcoplasmic reticulum. Delineation by lanthanum acting as a fortuitous tracer and in situ negative stain. J Cell Biol 59, 254–260.

West M, Zurek N, Hoenger A, Voeltz GK (2011). A 3D analysis of yeast ER structure reveals how ER domains are organized by membrane curvature. J Cell Biol 193, 333–346.

Wiest DL, Burkhardt JK, Hester S, Hortsch M, Meyer DI, Argon Y (1990). Membrane biogenesis during B cell differentiation: most endoplasmic reticulum proteins are expressed coordinately. J Cell Biol 110, 1501–1511.

Zankel A, Kraus B, Poelt P, Schaffer M, Ingolic E (2009). Ultramicrotomy in the ESEM, a versatile method for materials and life sciences. J Microsc 233, 140–148.